

Scintillator Testing for Use in the Pre-Shower Calorimeter

D. Keller¹, M. Yurov², K. Hicks¹, S. Stepanyan²

¹ Ohio University, Athens, Ohio 45701 USA

² Jefferson Lab, Newport News, VA 11973 USA

May 28, 2009

Abstract

Studies were done to test various types of scintillator and wave length shifting fibers for the construction of the Pre-Shower Calorimeter (PCAL). A cosmic ray test was done using various fiber and scintillator combinations to find the greatest light yield. A ^{90}Sr source was then used to test each combination and to confirm earlier findings. Further studies looked at the effects that bubbles and air gaps in the glue had on the measured light yield. Final selection of the scintillator type and wave shifting fiber will be based on the performance, assembly requirements, and price estimates. The results found here indicate that the FNAL through-hole scintillator design and the KURARAY multi-clad wave-length shifting fiber, along with careful gluing, give the best light output under the current testing configuration.

Contents

1	Introduction	2
2	Procedures	2
2.1	Cosmic Rays Test Setup	4
2.2	Test with ^{90}Sr Setup	6
3	Analysis and Results	8
3.1	Photo-electron Results	8
3.2	Cosmic Ray Results	9
3.3	Results of Tests with ^{90}Sr	10
3.4	Additional Tests with ^{90}Sr	13
4	Conclusions and Future Plans	17

List of Tables

1	Cosmic Ray Data	9
2	^{90}Sr Test Data	12
3	Small Scintillator Test	13

1 Introduction

The CLAS12 detector will include a pre-shower calorimeter (PCAL) with similar geometric design and readout scheme as the present CLAS electromagnetic calorimeter (EC). At higher energy the PCAL can provide additional accuracy for energy and position measurements of the electromagnetic shower. For example the current CLAS forward EC will not have the resolution to differentiate a two photon cluster from a high energy π^0 decay due to the close proximity of the two photon clusters on the EC plane. The Pre-Shower calorimeter with increased granularity can be used to resolve these close hits. The geometry of the Pre-Shower calorimeter, like the current EC, will consist of alternating layers of lead and scintillators forming a stack arranged in a near equilateral triangle. Each consecutive layer would consist of scintillators running parallel and sitting 120° to the previous layer. These three views of the triangle form a three stereo readout system. Light from each scintillator is conveyed to the photo-detector with 1 mm diameter green wave-length shifting fibers (WLSF) that runs through the scintillator. It has been proposed that instead of using the straight grooves to seat the fiber on the surface of the scintillator, that a through-hole inside the scintillator could be used. The fiber would then be fully enclosed in the scintillator after gluing unlike the grooved method. The procedure of gluing the fiber into the holed scintillator has not yet been investigated. In addition the light yield for the holed scintillator has not yet been tested in comparison to the grooved scintillator. In this report results are presented for the test measurements of the holed scintillator in comparison to the grooved scintillator with various fibers as well as a look at the effects of gluing on the light yield for the holed scintillator. The intention of these studies is to optimize the overall light collection and resolution while regulating reconstruction error of the pre-shower calorimeter.

2 Procedures

Setup and measurements were preformed in the semi-clean room in the EEL building of JLAB. The 4 meter long dark box in room 125 was used to control background light interference. The box contains a small sliding cart with a test PMT fastened to it. This made it convenient to change out various scintillators. The test scintillators with fiber were secured inside the box and

tested one by one. The light readout end of the test fiber was glued to a black plastic holder that fits securely to make an optical interface with the test PMT. For best optical contact, the surface of the fiber holder and the fiber were sanded and polished after being glued into holder, then cleaned and coupled to the PMT with BICRON BC-630 optical grease, Fig. 1. The fiber runs approximately 10 cm from the end of the scintillator to the holder and then to the photo-cathode of the test PMT. The test PMT was installed inside a black plastic housing with a thin μ -metal shield inside. The back end of the housing tube has an end-cap with connectors for the HV and signal cables. The test PMT and the trigger PMT are on the same axis as the scintillator. The scintillator end, opposite to the fiber, is connected to the trigger PMT.



Figure 1: Fiber Holder with fibers

A radiation test with a ^{90}Sr source was used to test each scintillator and fiber combination. In addition, a cosmic ray test was performed on the groove and hole combinations to confirm results.

The prior study in [1], found that a 1.5 mm fiber has a 25% greater light yield than a 1 mm diameter fiber, and a 2 mm fiber had a 40% greater light yield. The results also showed that a multi-clad fiber has about a 20% greater light yield than a single clad. Also the Bicron G91A 1mm single clad fiber had about 10% less light yield than the Kuraray 1 mm single clad Y11. In all of these former studies only a grooved scintillator was used.

The fibers used in all the following studies are Bicron G91A 1 mm multi-



Figure 2: Setup in Dark Box

clad and Kuraray Y11 1 mm multi-clad.

A set of measurements were previously carried out at different High Voltage settings for the test PMTs (gain studies). The purpose of these measurements was to find the operating HV settings before taking the actual data. A ratio of 10 channels of ADC per 1 MeV energy deposition was chosen to be within the dynamical range of the ADC. Because the test PMT is optically coupled with one scintillator strip (4.5 cm by 1 cm) at a time, cosmic ray collection is relatively slow. Minimum Ionizing Particles (MIP) with a vertical trajectory would deposit about 2 MeV for a single scintillator strip. The ADC response to MIPs was studied for different high voltage (HV) settings on the test and trigger PMTs.

2.1 Cosmic Rays Test Setup

The detector was setup with an additional scintillator counter, PMTs, Fast Bus crate electronics and the data acquisition system. The counter is a PMT connected to a small extension of scintillator which was mounted approximately 10 cm above the test scintillator. The test scintillator is cleaned and polished on one side to fit flush against a light guide leading to the trigger PMT. The fiber comes out of the opposing side into the fiber holder, which is also sanded and polished so that it will fit flush against the test PMT. Each optical connection is coupled with BICRON BC-630 optical grease. The fiber is glued to the scintillator with BICRON BC-600 optical glue. This setup is

specific for the selection of cosmic rays with primarily vertical trajectories.

The signals from the trigger PMT and the PMT connected to the scintillator counter were split in two. The trigger was setup with a coincidence of the second split signal between the scintillator counter and the trigger PMT so a Cosmic ray particle must traverse the counter and the test scintillator to trigger the acquisition.

Discriminated pulses (LeCroy 4413 16CH discriminator, initially the threshold was set to 30 mV) were fed into the logic circuit (Model 755 Quad Four-Fold Logic Unit). The output signal of the logic unit was used as a gate for the ADC module. Delay cables were used to time the second split signals going to the ADC LeCroy to fall within the gate. CODA was used as the interface software to the data acquisition. The CAEN NUCLEAR Model A1532 SY high voltage supply and discriminator were controlled with Epics software. A schematic of the setup can be seen in Fig. 3.

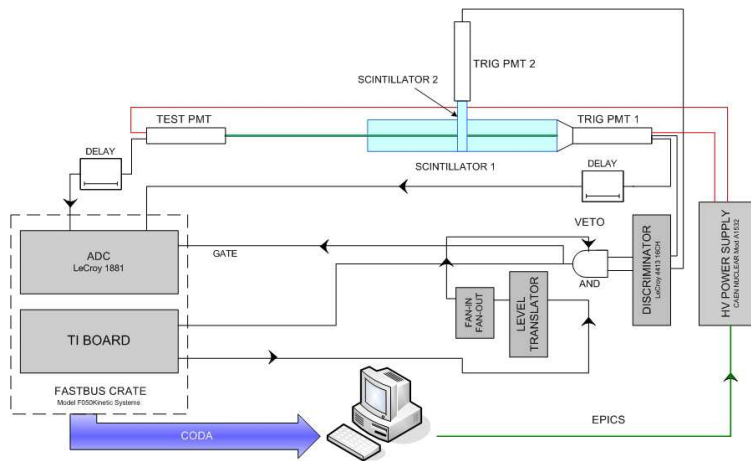


Figure 3: Schematic Setup of Cosmic Ray Test Hardware

There were several thousand events taken for each type of test scintillator. In the first test there were eight scintillators: four with grooves, 2 with Bicron fibers and 2 with Kuraray fibers, then four with holes, 2 with Bicron fibers and 2 with Kuraray fibers. The second set of each is simply for confirmation. Each test scintillator was 20 cm in length and 4 cm in width.

2.2 Test with ^{90}Sr Setup

The radiation test setup had the exact same configuration as the cosmic ray setup except there was only the trigger and test PMT with no counter on top. The coincidence was set to one and the threshold for the trigger PMT was set to 50 mV. A Strontium-90 β source is positioned on top of the scintillator. Strontium decays to ^{90}Y which has a β decay with a maximum energy of 2.28 MeV. The maximum energy deposited in the test scintillator fiber combination is approximately 2 MeV. A schematic for the setup can be seen in Fig. 4.

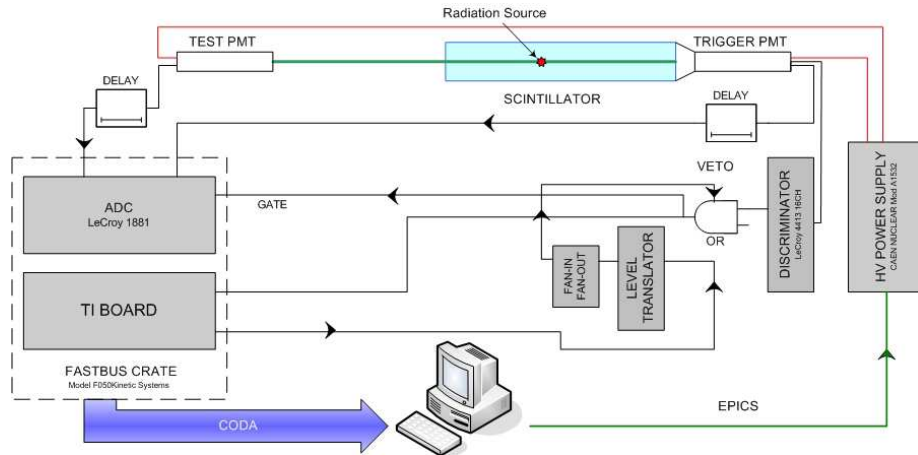


Figure 4: Schematic Setup of Radiation Test Hardware

For the first test (to determine the difference in yield for the grooved and the holed scintillator) the source was positioned roughly 1 cm away from the middle, where the fiber passes through, and roughly three fourths the way down the length of the 20 cm scintillator.

A series of measurements with ^{90}Sr were performed to confirm the findings of the original cosmic ray test as well as to test the difference of the Kuraray and Bicron fibers in the through-hole scintillator. Also a set of tests were done to study the relative yields down the length and across the width of the scintillator. Finally there were various tests to learn about the effects of gluing on the light yield. The results of each test can be understood in a relative ADC comparison of light yield and the number of photo-electrons, which required a photo-electron statistics study.

At the first stage, the position of the Single Photo-Electron (SPHE) peak

was identified at nominal HV settings. This was done by decreasing the amount of light going into the test PMT using the amplitude control of the signal going to a LED inside the dark box enclosure. The peak was attributed to the SPHE distribution when only a single peak remained in the spectrum above the pedestal and further decrease of the light only changed the amplitude of the peak but not the position. These tests were done at 4 values of LED amplitude from highest to smallest, at the same nominal HV used in the cosmic ray test.

In the next two stages, a series of measurements were taken for 4 different HV settings using the particular value of LED amplitude for which the SPHE regime was achieved. The purpose of these measurements was to minimize uncertainties in the SPHE position since it was very close to the pedestal at nominal HV. In the third stage, a gain curve was obtained.

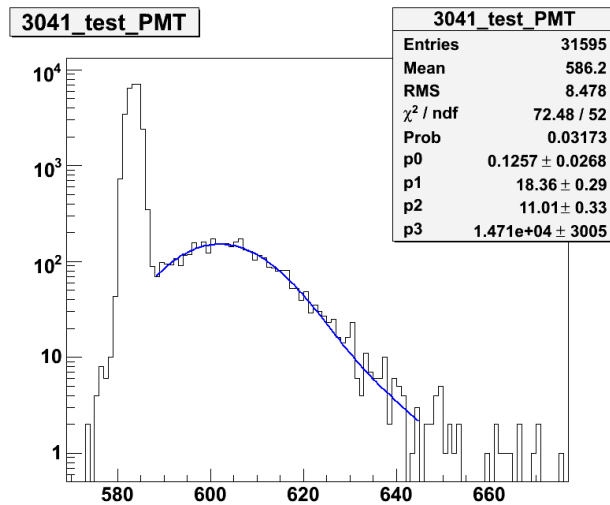


Figure 5: Position of Single Photo-electron Peak

3 Analysis and Results

3.1 Photo-electron Results

To determine the position of the (SPHE) peak, which is used to convert channels of the ADC to the number of photo-electrons, measurements with LED were used. The first photo-electron peak was found using the amplitude control of the signal going to a LED inside the dark box enclosure. These tests were done at 4 values of LED amplitude from highest to smallest, at the same nominal HV used in the cosmic ray test. The mean of the Gaussian fit after pedestal subtraction represents the position of the single photo-electron peak. For the first set of trials the result came out to be 18.36 ± 0.29 ADC channels for one photo-electron seen in Fig. 5. If anything changes in the electronics, such as ADC or HV, then this value will change as well, so it is important to recheck it at different stages of the experiment.

The analysis of the photo-electron statistics is described in [6]. Each ADC spectrum can be fit with a convolution of the Gaussian distribution $G_i(n_{ch})$ of ADC channels and the Poisson probability $P_i(n_{pe})$ for a given number of photo-electrons. This convolution fitting was done in the initial radiation tests. The results are given in Table 2. The relation can be written as,

$$A = C \sum_i P_i(n_{pe}) G_i(n_{ch}) \quad (1)$$

$$P_i(n_{pe}) = \frac{n_{pe}^i e^{-n_{pe}}}{i!} \quad (2)$$

$$G_i(n_{ch}) = \frac{1}{\sigma_1 \sqrt{i}} e^{-(\frac{n_{ch} - (a_1 + (i-1) \cdot a_0)}{\sigma_1 \sqrt{2i}})^2} \quad (3)$$

The summation of Eq. (1) is over the possible number of photo-electrons in the spectrum, i . The coefficient C represents the overall normalization, while n_{pe} is the average number of photo-electrons. Eq.(3) has n_{ch} as the pedestal subtracted ADC channel number. The parameters a_1 and σ_1 are the position and the standard deviation of the single photo-electron peak in the units of ADC channels. The a_0 parameter is the distance between two adjacent photo-electron peaks in the units of ADC channels. The fit parameters used in the initial radiation test were C , n_{pe} , and a_0 .

3.2 Cosmic Ray Results

The cosmic ray data was taken for eight different runs at roughly 20 thousand events per run. In the analysis there was a selection cut on the data keeping only the events with a trigger that comes from primarily vertical cosmic rays. This is done by keeping the events seen in the test and trigger PMTs that correspond to events in the counter PMT that are localized around the peak of the ADC distribution. This ensures that the remaining counts are mostly from minimum ionizing particles with a vertical trajectory. The ADC distribution from the test PMT is compared to the trigger PMT. This can be seen in Fig. 6. The top left plot shows the scintillator counter ADC distribution and the selection cuts used. In the top right plot the ADC distribution for the test PMT is along the Y-axis. The areas with a higher density of points designates the relative coincidence between these two PMTs. This high density area can be isolated and fit with a Gaussian to find the mean, which is seen in the bottom two plots. One can then take this mean, subtract the pedestal, and divide by the number of photo-electrons per channels of ADC to get the final yield in terms of the photo-electron number.

This procedure was done for all eight of the grooved and holed scintillators, giving the results seen in able Table 1. The table lists the type of scintillator and fiber in the far left column where B is for Bicron and K is for Kuraray fibers. G is for grooved and H is for through holed. There were two trials on each type listed as 1 and 2. The run number is listed with the ADC mean from a Gaussian fit after the pedestal subtraction. The number of photo-electrons are listed in the right column.

Table 1: Cosmic Ray Data

Type	Run #	ADC mean	# photo-electrons
B1G	3033	236.4 ± 0.1	12.87 ± 0.01
B2G	3053	205.5 ± 0.2	11.19 ± 0.01
K1G	3047	307.9 ± 0.2	16.77 ± 0.01
K2G	3049	304.5 ± 0.2	16.58 ± 0.01
B1H	3056	364.1 ± 1.6	19.83 ± 0.09
B2H	3129	327.2 ± 0.3	17.82 ± 0.02
K1H	3061	294.9 ± 0.4	16.06 ± 0.02
K2H	3077	312.7 ± 0.3	17.03 ± 0.02

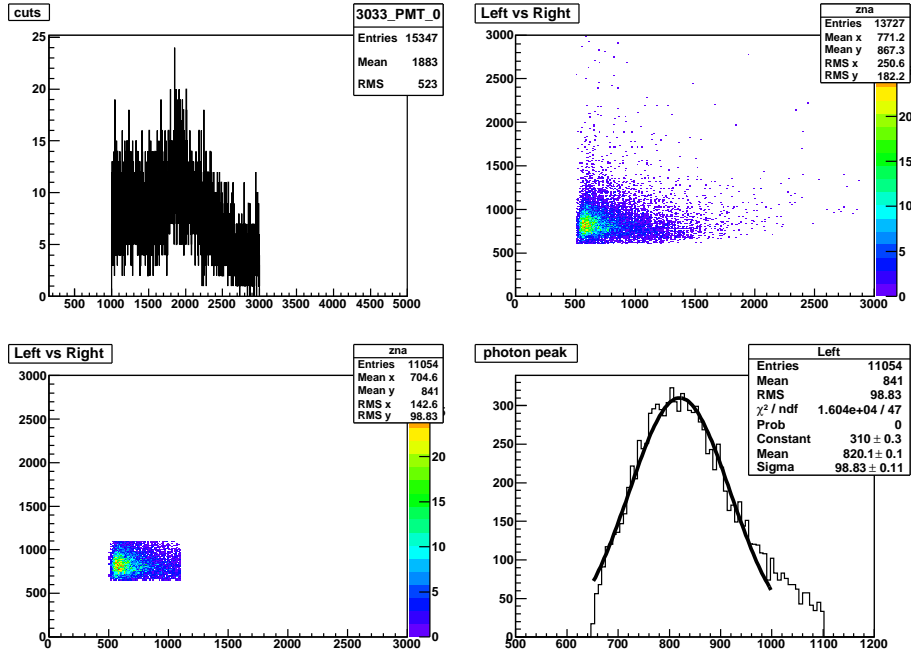


Figure 6: Top left: Cosmic ray trig for MIP of vertical trajectory; top right: ADC distribution Right vs Left. Bottom left: Photo-peak and fit; bottom right: cuts used.

3.3 Results of Tests with ^{90}Sr

A test with ^{90}Sr was completed for each of the scintillators listed in Table 1. This was done to confirm the findings. The analysis for this data is slightly different from before. A ^{90}Sr data set was taken with eight different runs at roughly 250 thousand events per run. The first step in the analysis was to compare the ADC distribution from the test PMT to that of the trigger PMT. Because the trigger is setup for coincidence of one, the test ADC distribution and the trigger ADC distribution overlap can be seen in the 2D-histogram in Fig. 7. This high density area of events can be sliced along the trigger ADC distribution in equal bins and projected on to the test PMT axis. Each projection can then be fit with either a convolution of a Poisson and a Gaussian, which is more systematically correct, or just a Gaussian for simplicity. Because the measurements were carried out using a β -source, the ADC distribution of the test PMT will correspond to the

part of the β spectrum that was selected by the trigger PMT. The selection naturally depends on the optical connection between the trigger PMT and the scintillator, the trigger PMT HV setting, and the discriminator threshold. The part of the energy spectrum of interest is the known saturation point which can be seen at the tail of the trend (roughly 2 MeV), see Fig. 7. After the bin range is chosen for the trigger PMT, the ADC distribution and the test PMT spectra are fit. One can see that with the increase of the trigger PMT ADC channel number, the average number of photo-electrons in the test PMT increases and ultimately reaches a maximum value. This maximum level at the end of the spectrum is the saturation point of 2 MeV. One then uses this end point to fit a horizontal line and compares the saturation point to resolve the greatest light yield between the various scintillators.

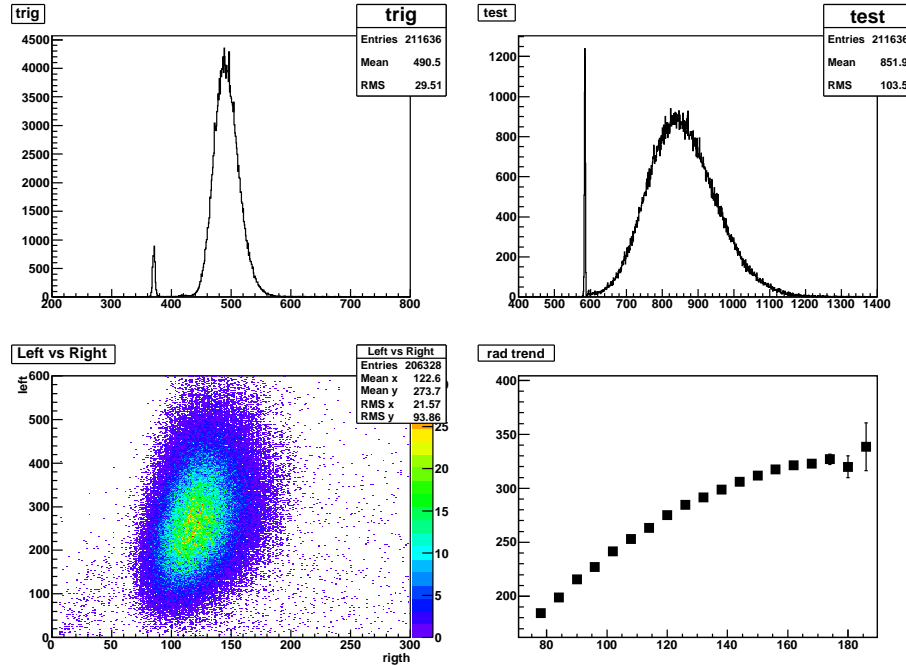


Figure 7: TOP: Trigger and Test PMT ADC distribution for run 3050, BOT-TOM right: Trigger PMT ADC vs Test PMT ADC: , left: Trend of sliced ADC mean after fitting.

This procedure was done on all eight of the grooved and holed scintillators, giving the results seen in Table 2. Again, the table lists the type of scintillator and fiber in the far left column where B is for Bicron, K is for Kuraray fibers,

G is for grooved and H is for holed. There were two trials on each type listed 1 and 2. The run number is listed with the ADC mean from a Gaussian fit after the pedestal subtraction. The number of photo-electrons are listed in the right column.

Table 2: ^{90}Sr Test Data

Type	Run number	ADC mean	photo-electrons
B1G	3043	276.2 ± 0.1	13.17 ± 0.4
B2G	3052	205.9 ± 0.2	11.11 ± 0.3
K1G	3048	319.6 ± 0.2	14.72 ± 0.2
K2G	3050	320.6 ± 0.2	14.64 ± 0.3
B1H	3059	351.0 ± 0.2	15.91 ± 0.5
B2H	3065	396.7 ± 0.1	19.82 ± 0.3
K1H	3060	295.1 ± 0.3	13.76 ± 0.4
K2H	3063	343.9 ± 0.3	14.58 ± 0.3

The number of photo-electrons in Table (2) were not calculated as a direct conversion from the ADC, as was done in the cosmic ray data. Instead they were calculated using fits from the convolution of Poisson and Gaussian seen in Eq. (1). The ADC mean is from the Gaussian fits. This gives a means to test the capacity of the convolution against the standard method of fitting with the Gaussian. The results of this comparison are quite clear. The convolution needs relatively higher statistics to consistently make a good fit compared to the Gaussian fit alone. Because of the nature of our study it is enough to find the mean in ADC from a simple Gaussian fit. Ultimately it is only the relative light yield that is needed to deduce the better efficiency when comparing the various scintillator and fiber combinations.

These results indicate that the holed scintillator gives slightly greater light yield than that of the grooved. The difference overall does not appear to be significant. During the setup of the hole scintillator it was observed that gluing the fiber in the hole while completely filling the hole with optical glue is an issue. This challenge is not applicable to the grooved scintillator.

Because it was difficult to conclude anything about the difference in Bicron and Kuraray fibers in the holed scintillator, a separate test was done with no other variations. Two similar holed scintillator strips of 4 cm by 20 cm were cut and glued very carefully. The only difference was that one fiber was Bicron and the other was Kuraray. The position of the source was placed at the same cross hairs measured from the test PMT end of the scintillator

(longitudinally) and the open end of the dark box (transversely). The error in position was estimated to be less than ± 0.25 mm at each measurement. The Kuraray fiber gave a 20% greater yield than the Bicron.

3.4 Additional Tests with ^{90}Sr

After looking at some of the initial results it was decided to perform some retests to confirm the findings and to establish more details. Four small scintillators were cut with dimensions of 4 cm in width and 3.75 cm in length. The fiber used had a minimal length of 6 cm. These components were minimized to reduce the likelihood of gluing inconsistencies and fiber damage effects. One of these small scintillators was glued with a Bicron fiber and one with a Kuraray fiber with very careful gluing. Another one was glued with Kuraray with a well formed bubble inserted to test for the effects of bubbles on the yield. Finally a scintillator was used with no glue at all to test the extreme case. The results can be seen in Table 3. The relative light yield can be seen from the saturation point in each case in Fig. 8.

Table 3: Small Scintillator Test

Type	Run #	ADC mean	# photo-electrons
Bicron	3043	192.6 ± 0.40	9.68 ± 0.02
Kuraray	3052	238.9 ± 0.40	12.01 ± 0.02
Bubble	3048	217.9 ± 0.38	10.94 ± 0.02
No-Glue	3050	139.8 ± 0.37	7.02 ± 0.02

Measurements were done to study light yield dependence on the transverse position of the radiation. Scintillators of various length were marked with equal spaced cross hairs to place the ^{90}Sr source to test the relative yield at each position.

The initial test was on a 4 cm wide by 20 cm long scintillator strip. This test was performed across the width of the scintillator strip at seven different points. The width test was done by placing the radiation source at each point along the width for several hundred thousand events. The results of this test are shown in Fig. 9. The general trend of greater yield close to the fiber is visible. To study the resolution, a test with more points was required. In addition it was desired to have some data with various widths of the available scintillator in case the selected widths for PCAL fabrication might change. In the ideal case for the final selected hole position and width

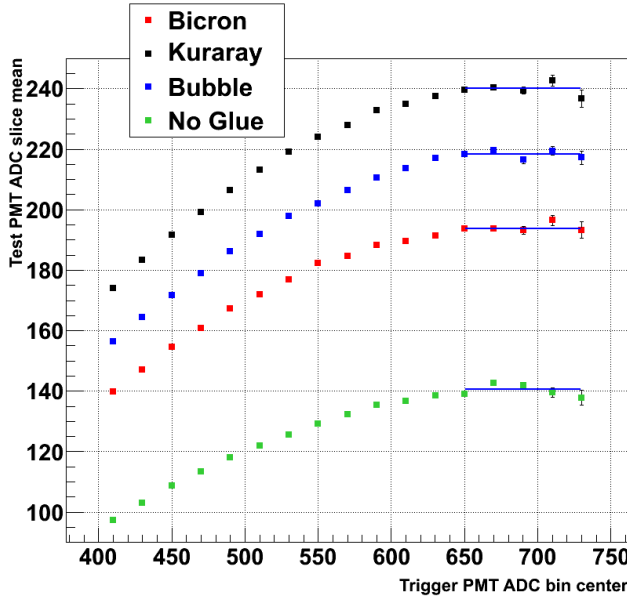


Figure 8: Small Scintillator Tests Yield

of scintillator, a semi-flat even distribution of light collection is needed to regulate and minimize the PCAL systematic error.

The same test was conducted on a scintillator strip that was 5 cm by 30 cm. Each point was measured very carefully and drawn on the scintillator as a cross hair. The source was setup with wire pointers on each orthogonal side to match the cross hairs for accurate positioning. There were 14 points taken along the width and roughly 500k events were taken at each point. The results can be seen in Fig. 10.

The overall expected trend is visible in both Fig. 9 and Fig. 10 with the greatest yield closest to the fiber. After fitting with a Gaussian one can notice that the σ parameter is nearly 50% different, which is likely due to the different widths of the scintillators seen in Fig. 11 and Fig. 12. For the sake of looking at the possible overall yield curve in relation to hole position, the 5 cm wide strip was used.

In the original setup of the 4.5 cm scintillator with two holes, the hole positions were placed at 11.25 mm and 33.75 mm from one side of the strip. The fit in Fig. 12 was used to project what the profile of the 4.5 cm wide strip with two holes might look like. The sum of yields is shown by the yellow curve in Fig. 13. From this projection one can see a gain in yield from the

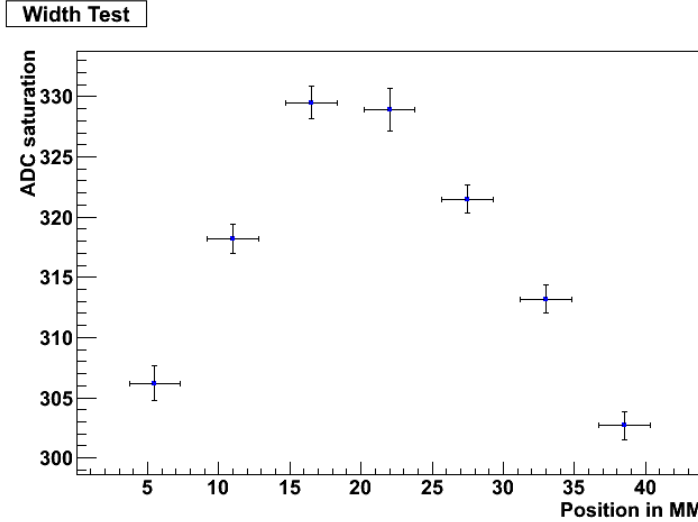


Figure 9: First Test Across Scintillator Width (4 cm)

edge of the strip to the center of more than 40%. To regulate the error in the PCAL this gain should be minimized. By moving the holes out farther one can get a more even distribution over the width of the strip. This is seen in the yellow curve in Fig. 14.

These projections are based on the Gaussian fit parameter σ from the 5 cm wide strip which is expected to differ from the 4.5 cm strip. The different proximity of the fiber to the edge is also expected to change the shape of the dependence. However, under the given assumptions these results indicate that care should be taken to study the most error efficient configuration of the two holed 4.5 cm scintillator.

After the width test was done, a longitudinal test was conducted on the same 5 cm by 30 cm scintillator strip. Again each point was measured very carefully and drawn on the scintillator as cross hairs and the source was setup with wire pointers on each orthogonal side to match the cross hairs for accurate positioning. There were 10 points at 3 cm steps. The offset from the middle of the scintillator was approximately 1 cm. This test can be used to measure attenuation of the fiber scintillator combination.

In addition there is a need to obtain some type of quality test. It is thought that the longitudinal test can be used to test the quality of the gluing down the length of the fiber in the scintillator. Once each of the

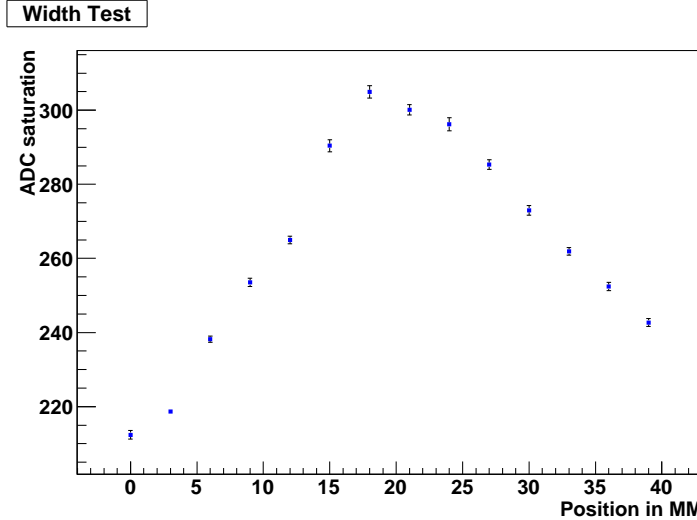


Figure 10: Second Test Across Scintillator Width (5 cm)

PCAL 4 m long scintillators have been cut and glued with fiber in place they should be tested to have the appropriate attenuation trend without effects of bubbles or air pockets which could disrupt the trend. The results of the measurements can be seen in Fig. 15.

The longitudinal procedure was repeated over a larger 100 cm long scintillator with 33 points. This can be seen in Fig. 16.

It is expected to see a general trend over the length of the scintillator that is governed by exponential attenuation effects. The effects can be seen in both the resulting longitudinal tests, but one can also see an incredibly fast drop off at 5 cm from the end of the fiber not due to attenuation. The time it takes to collect data is comparably long in this procedure because the farther the source is from the trigger PMT the more difficult it is to gather data strictly triggered by the radiation. The rapid falloff seen at the last points farthest from the test PMT seen in Fig. 16, is thought to be due to the solid angle of the source extending beyond the termination point of the fiber on the trigger end. The trend is consistently seen at less than 5 cm from the trigger end of the scintillator.

An exponential is used to fit the points giving a slope parameter of about 0.004. The expected slope parameter is 0.0033 due to the attenuation length of 300 cm. Attenuation takes the form e^{x/l_a} , where l_a is the attenuation

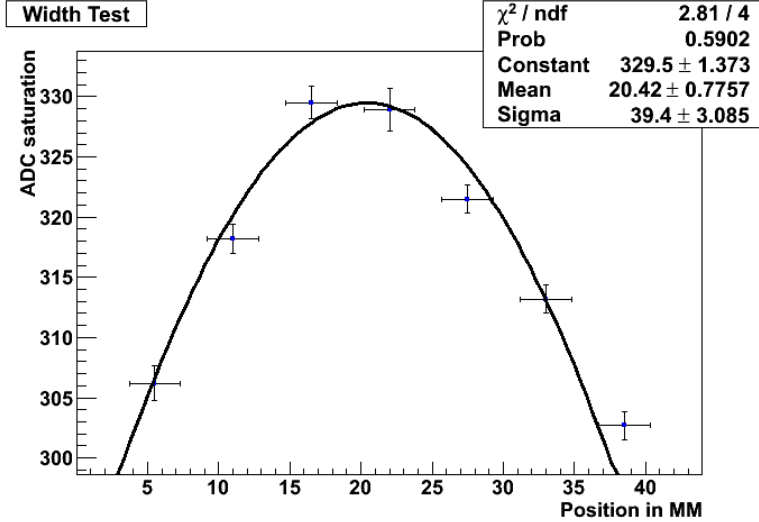


Figure 11: Fit to First Test Across Scintillator Width (4 cm)

length. This fit is seen in Fig. 17.

4 Conclusions and Future Plans

One can see from the comic ray test and radiation test that the through-holed scintillator gives an overall greater light yield than the grooved scintillator. However this conclusion seems to be directly dependent on the quality of gluing in the holed scintillator. The holed scintillator is more challenging to glue than the grooved and more studies should be done to achieve an efficient method. After careful gluing, some retests were performed to find that Kuraray does indeed give a greater light yield than Bicron in the holed scintillators. Based on the two trials there was a 20-30% greater yield from Kuraray. This implies that the data for Kuraray holed in Table 1 and Table 2 is adversely affected by bad gluing. Through the course of these studies it is evident that if the gluing in the through-holed scintillator is not studied and understood it could inadvertently reduce the available light yield in an irregular way, creating a fluctuation in the systematic error.

Additional tests were performed to gain some information about the width and length trends in yield that can be used to study the resolution of the detector. The width test was used to study the two hole scintillator profile.

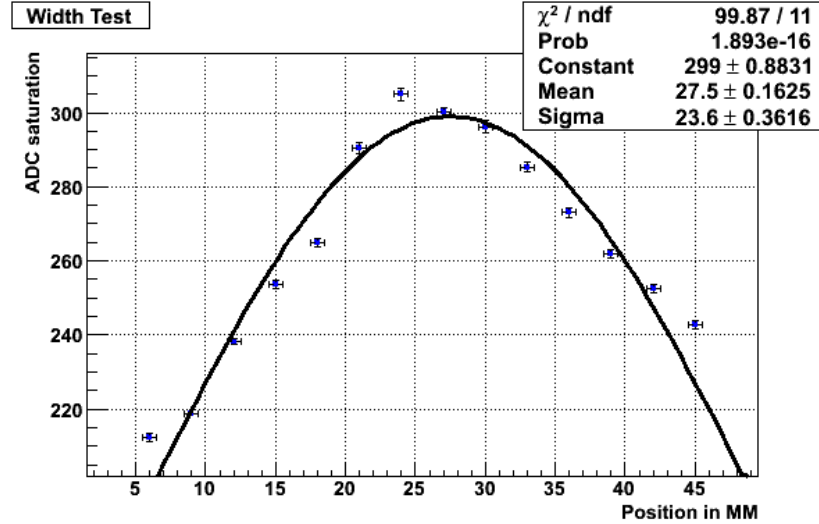


Figure 12: Fit to Second Test Across Scintillator Width (5 cm)

Under the parameters found from the 5 cm wide strip the 4.5 cm wide strip holes appear to have been placed too close in the original design. The yield summing effects in the 4.5 cm scintillator of the two fibers should be studied further.

The longitudinal test was thought of as a possible quality test. An exponential trend is seen in the result but only over part of the scintillator. The fit gives an attenuation length that is not in direct comparison with the known attenuation length. This implies a further look at the systematics involved. In addition the falloff near the end of the fiber reduces the capacity to study glue quality at this end. Moreover, the time it takes to gather the data for the long scintillators radiation test is considerable and may not be reasonable for a quality test on multiple scintillators.

Two Hole Profile

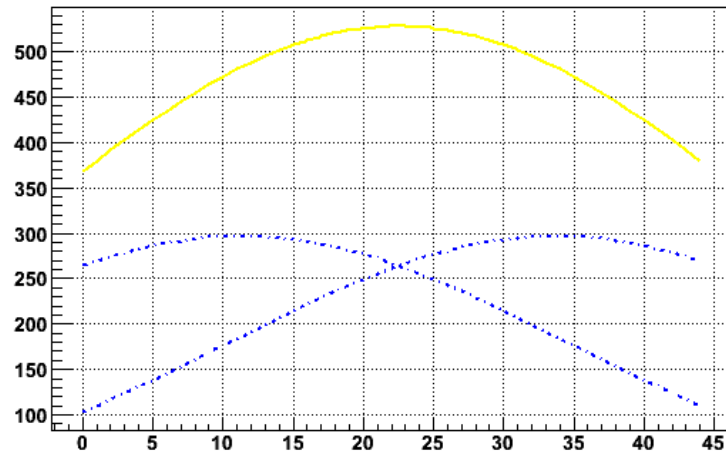


Figure 13: Projection of the 4.5 cm profile with 2 holes positioned at 11.25 cm and 33.75 mm

Two Hole Profile

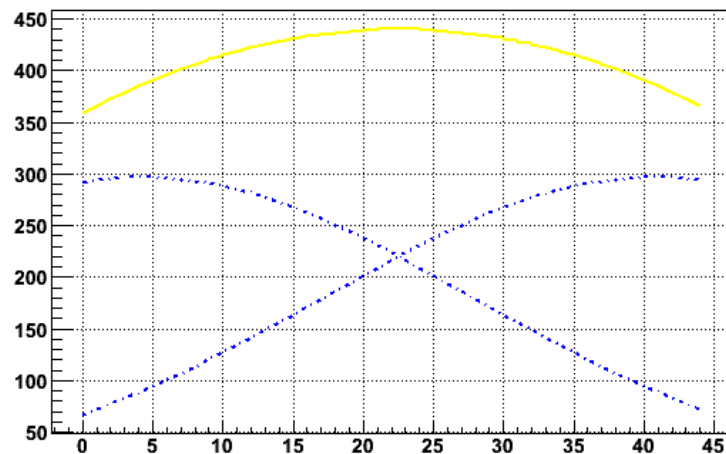


Figure 14: Projection of the 4.5 cm profile with 2 holes moved to 4.25 cm and 40.75 cm

Longitudinal Test

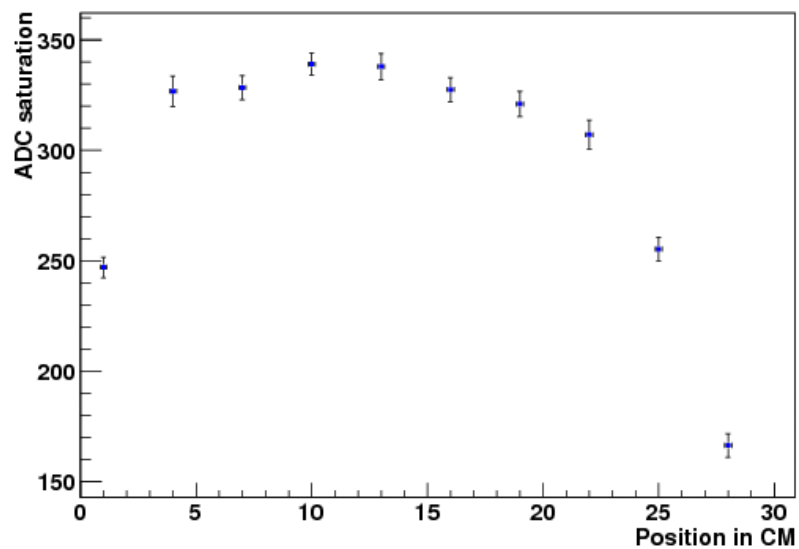


Figure 15: First Longitudinal Test (30 cm)

Longitudinal Test

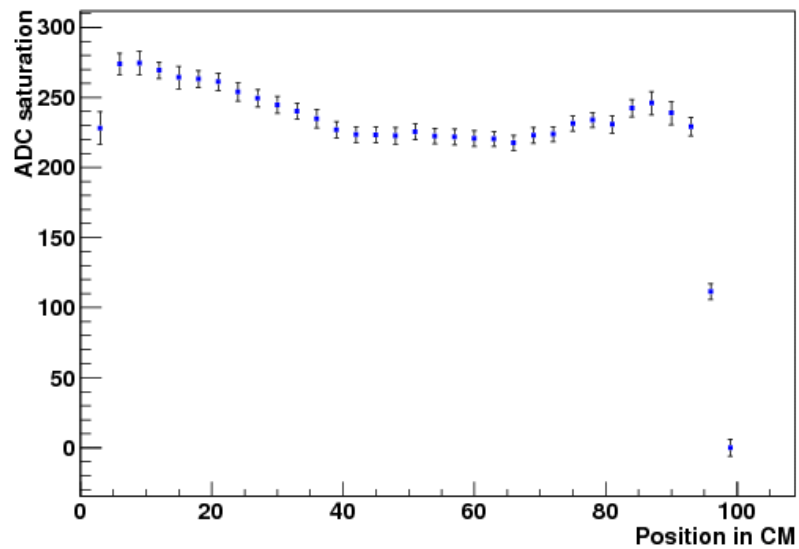


Figure 16: Second Longitudinal Test (100 cm)

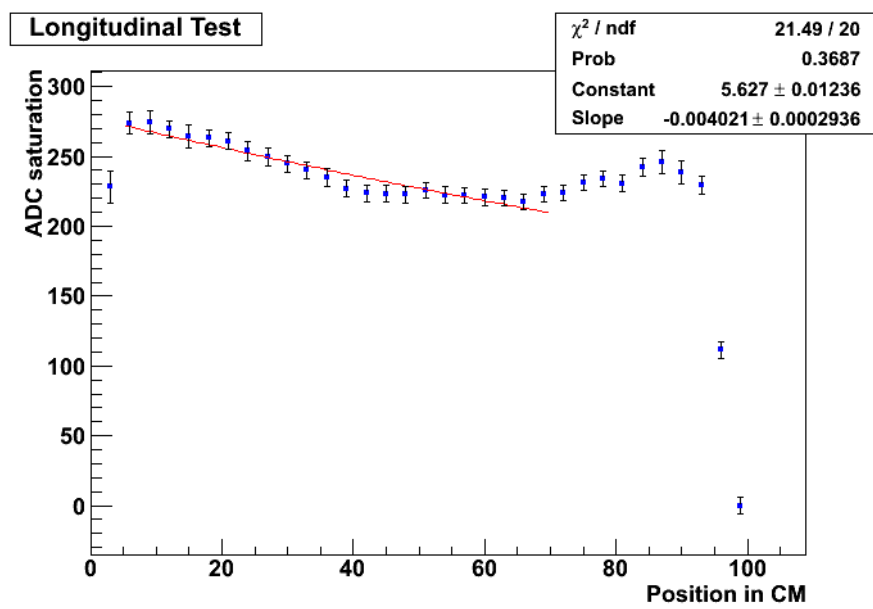


Figure 17: Second Longitudinal Test exponential fit

APPENDIX

List of Figures

1	Fiber Holder with fibers	3
2	Setup in Dark Box	4
3	Schematic Setup of Cosmic Ray Test Hardware	5
4	Schematic Setup of Radiation Test Hardware	6
5	Position of Single Photo-electron Peak	7
6	Top left: Cosmic ray trig for MIP of vertical trajectory; top right: ADC distribution Right vs Left. Bottom left: Photo-peak and fit; bottom right: cuts used.	10
7	TOP: Trigger and Test PMT ADC distribution for run 3050, BOTTOM right: Trigger PMT ADC vs Test PMT ADC: , left: Trend of sliced ADC mean after fitting.	11
8	Small Scintillator Tests Yield	14
9	First Test Across Scintillator Width (4 cm)	15
10	Second Test Across Scintillator Width (5 cm)	16
11	Fit to First Test Across Scintillator Width (4 cm)	17
12	Fit to Second Test Across Scintillator Width (5 cm)	18
13	Projection of the 4.5 cm profile with 2 holes positioned at 11.25 cm and 33.75 mm	19
14	Projection of the 4.5 cm profile with 2 holes moved to 4.25 cm and 40.75 cm	19
15	First Longitudinal Test (30 cm)	20
16	Second Longitudinal Test (100 cm)	20
17	Second Longitudinal Test exponential fit	21

References

- [1] G. Asryan, N. Dashyan, H. Voshanyan, V. Burkert, D. Kashy, S. Stepanyan, M. MacCormick, P. Rosier, C. Salgado, M. Khandaker, K. Hicks, K. Giovanetti, Pre-shower calorimeter for the CLAS12 detector 2007-007.
- [2] T.C. Awes, F.E. Obenshain, F. Plasil, S. Saini, S.P. Sorensen and G.R. Young, Nucl. Instr. and Meth. A311 (1992).
- [3] Particle Data Group, Phys. Rev. **D54** (1996) 52.
- [4] M.G. Bekishev, V.N. Ivanchenko, Nucl. Instr. and Meth. A361 (1995).
- [5] *The Physics of Particle Detectors*, D. Green, Cambridge Monographs on Particle Physics, Nuclear Physics and Cosmology (2000).
- [6] V. Burkert, CLAS-NOTE 1992-008.